## SCIENCE CHINA Chemistry



·ARTICLES·

October 2025 Vol.68 No.10: 5001–5006 https://doi.org/10.1007/s11426-025-2637-2

# Barbiturate-containing macrocycles: synthesis, structure and anion recognition through anion-carbonyl interactions

Jun Zhu<sup>1</sup>, Xu-Dong Wang<sup>1\*</sup>, Yu-Fei Ao<sup>1,2</sup>, Qi-Qiang Wang<sup>1,2</sup> & De-Xian Wang<sup>1,2\*</sup>

<sup>1</sup>Beijing National Laboratory for Molecular Sciences, CAS Key Laboratory of Molecular Recognition and Function Institute of Chemistry,

Chinese Academy of Sciences, Beijing 100190, China

<sup>2</sup>University of Chinese Academy of Sciences, Beijing 100049, China

Received January 23, 2025; accepted March 11, 2025; published online April 15, 2025

Anion-carbonyl interaction is a newly developed non-covalent bond, and its application as a driving force in supramolecular chemistry deserves exploration. Herein, a series of barbiturate-containing macrocycles were synthesized using macrocycle-to-macrocycle transformation or one-pot macrocyclization. Various structural conformations arising from the interplay of non-aromatic barbiturate and benzene rings through N–C rotations in solution were revealed. The macrocycles featuring carbonyl donors and acceptors resulted in unique self-assembly structures and host-guest complexes in the crystalline state. The [3+3] macrocycle 7a was applied as a host molecule to investigate the complexation with anions by  $^{13}$ C nuclear magnetic resonance (NMR) titrations, which showed selective binding towards malonate with an association constant of  $K_{a(1:1)} = 13.2 \pm 1.57 \text{ M}^{-1}$ . Multiple anion-carbonyl interactions between 7a and malonate were revealed by density functional theory (DFT) optimization of the complex.

barbiturate macrocycles, anion-carbonyl interactions,  $n\rightarrow\pi^*$  interactions, host-guest chemistry

Citation: Zhu J, Wang XD, Ao YF, Wang QQ, Wang DX. Barbiturate-containing macrocycles: synthesis, structure and anion recognition through anion-carbonyl interactions. Sci China Chem, 2025, 68: 5001–5006, https://doi.org/10.1007/s11426-025-2637-2

#### 1 Introduction

Non-covalent interactions form the fundamental basis for molecular recognition [1]. Supramolecular chemistry and in particular tailor-made macrocyclic compounds provide molecular models to probe the nature of new non-covalent interactions [2]. Indeed, supramolecular host macrocycles have advanced the development of novel non-covalent bonds including cation- $\pi$  interactions [3,15], halogen bonds [4,16], chalcogen bonds [5] and anion- $\pi$  interactions [6].

The attractive interactions between lone pairs of nucleophiles and carbon of the carbonyl group, also denoted as orthogonal multipolar or  $n\rightarrow\pi^*$  interactions are emerging non-covalent bonds in biological systems and the field of

chemistry [7]. Recent studies have highlighted the important roles of intramolecular carbonyl interactions in stabilizing the conformation of biomolecules and small molecules [8], modulating the reaction activity and selectivity [9], and influencing dynamic covalent equilibria [10]. Intermolecular  $n\rightarrow\pi^*$  interactions, though relatively underexplored, have demonstrated their potential as driving forces to induce selfassembly structure, host-guest complex and catalysis [11]. In advancing the concept of  $n\rightarrow\pi^*$  interactions, we recently reported a concept of anion-carbonyl interactions (X<sup>-</sup>···C=O interaction), the interaction between carbonyl and negativecharged anions [12]. DFT calculations based on imide-halide complexes as interacting models indicated a favorable binding energy of 10–50 kcal/mol between anion and imides in the gas phase, and electrostatic attraction and delocalization of halide lone pairs on the carbonyl antibonding orbitals

<sup>\*</sup>Corresponding authors (email: wangxd@iccas.ac.cn; dxwang@iccas.ac.cn)

are the primary contributions. Experimental evidence of anion-carbonyl interactions was provided through spectroscopic measurements and X-ray single-crystal analysis. However, the quantitative evaluation of anion-carbonyl interactions in solution was unsuccessful due to the significant reduction in the binding energy of single anion-carbonyl interaction by the solvation of anions. To enable the hostguest quantification driven by anion-carbonyl interactions in solution, and to provide a "pure" carbonyl donor model for anion-carbonyl interactions, we envisioned a series of novel macrocycles based on barbiturates as the building blocks for three key considerations: (1) barbiturate moiety is a nonaromatic six-membered ring with three carbonyl groups arrayed in a  $C_{2\nu}$ -symmetric manner, allowing the formation of superimposed  $\pi$ -holes or  $\pi^*$  orbitals at the central region, (2) various substituents could be introduced on the  $\alpha$ -position of the carbonyl groups, which provide chances to modulate the binding ability of carbonyl groups, (3) assembling of barbiturates into a convergent macrocyclic cavity (host) could provide cooperative carbonyl binding sites for accommodating guests.

#### 2 Results and discussion

To access the target macrocyclic molecules, two synthetic strategies were employed. As shown in Scheme 1, macrocycles 3 consisting of single-substituted barbiturates were prepared through a macrocycle-to-macrocycle transformation [11a]. The reaction of a macrocyclic precursor 1 with malonyl dichloride compound 2 produced the target macrocycles 3 in high yields (72%–84%). For the synthesis of macrocycles bearing geminal substituents on barbiturate rings, a one-pot strategy was applied starting from barbiturate derivatives 5 and 1,3-bis(bromomethyl)benzene 4. In the presence of sodium hydride (NaH) as the base and in dimethyl formamide (DMF) at 80 °C, the reaction between 4 and 5 proceeded efficiently to afford the [2+2] macrocyclic products of 6, [3+3] macrocycles of 7 and [4+4] macrocycles of 8 in 32%-45%, 20%-21%, and 6%-12% yields, respectively. On the other hand, the non-substituted macrocycle 3a was used as a starting reagent to react with benzaldehyde to quantitatively produce a styrene-substituted macrocycle 9. All the macrocyclic compounds were fully characterized with spectroscopic and elemental analyses (supporting information). All the macrocycles synthesized are crystalline compounds. High-quality single crystals were obtained and their structures were determined unambiguously by X-ray diffraction analysis.

The single crystal structures of [2+2] compounds **3a-3d**, **6a-6c** are shown in Figure 1 and Figures S1 and S2 (Supporting Information online) [13]. Various conformations showing dependence on the size of substituents were re-

Scheme 1 (Color online) Synthesis of the barbiturate-containing macrocycles.

vealed. The non-substituted and mono-methyl substituted macrocycles 3a [11a] and 3b adopt cone conformations. Other mono- or geminal-substituted macrocycles (3c-3d, 6a-6c) adopt distorted 1,2-alternate conformations, which afforded flat rhomboid cavities with two benzene rings flatly and two barbiturate rings vertically arrayed in an antiparallel manner, respectively. Here the distorted 1,2-alternate conformation differs from the classical 1,2-alternate calix[4]arene, where the four benzene rings adopt an up-up-downdown array. Since methylene bridges barbiturate and benzene respectively through C-N and C-C bonds, the unique distorted 1,2-alternate conformation may arise from C-N and C-C dipole interactions, and the steric hindrance of the substituents on barbiturate. Besides, the substituents in **3b–3d** owing to the asymmetric substitution nature adopt either cis- or trans-configurations relative to the macrocycle. For example, one methyl group of **3b** directs toward the macrocycle (in), and the other points outward (out), hence the methyl groups are *cis*-arrayed (in/out) (Figure 1a), whereas ethyl and benzyl groups of 3c (in/in) and 3d (out/out or in/in) show trans-configuration (Figures S1b and S2a, b). The crystal structures of larger macrocycles show increased size and flexibility in comparison with the [2+2] macro-

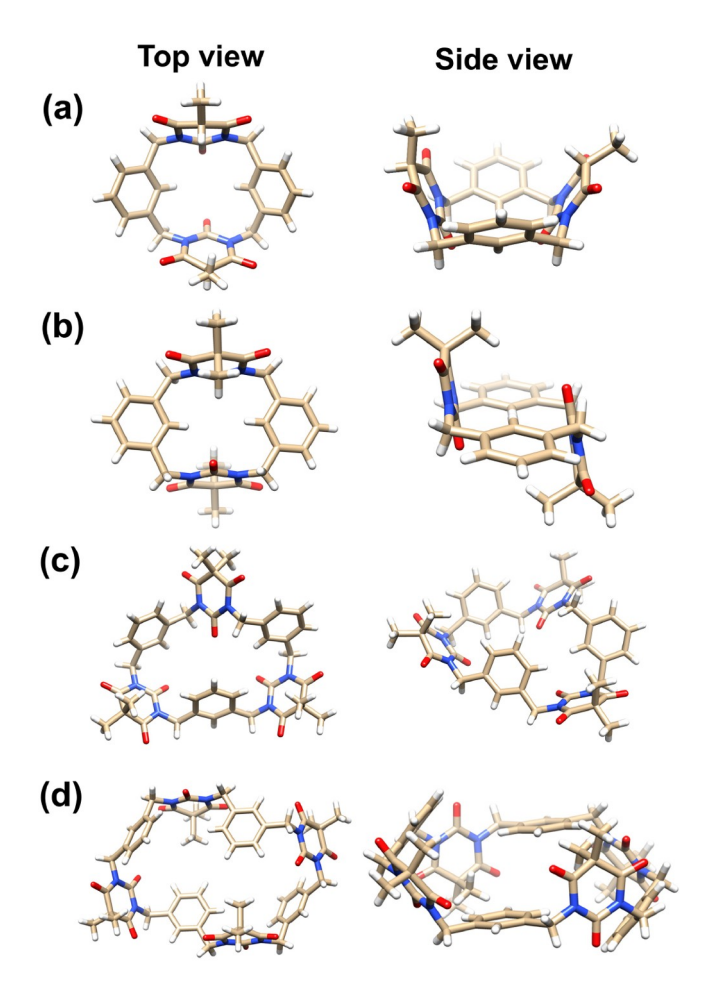


Figure 1 (Color online) Single crystal structures of 3b (a), 6a (b), 7a (c) and 8a (d). Color code: carbon, yellow; oxygen, red; hydrogen, white; nitrogen, blue.

cycles. For example, the [3+3] macrocycle 7a gives a twisted 1,3,5-alternate conformation and distorted cavity (Figure 1c), while 8a-8c show twisted 1,3,5,7-alternate conformations, forming distorted (8a) (Figure 1d) or rectangular (8b and 8c) cavities (Figures S1d and S2d) [13]. The macrocycle exhibits a significantly superimposed positive electrostatic potential ( $\pi$ -holes) over the central region of each barbiturate ring and negative potential concentrated on the carbonyl oxygens (Figure S13), could serve as a dual-functional building block, with the barbiturate ring as lone pair acceptor and carbonyl oxygen as lone pair donor. Intermolecular C=O···C=O interactions, following the Bürgi-Dunitz trajectory ( $d < \Sigma v dW$ ,  $\angle O \cdots C - O = 109^{\circ} \pm 10^{\circ}$ ), are general for all mono-substituted and geminal-methyl substituted [2+2] macrocycles 3a-3d and 6a, except for geminal-ethyl and -benzyl substituted macrocycles (6b, 6c, 8b, 8c) where the front and back surfaces of barbiturates are blocked by the larger groups (Figure S16). The C=O···C=O interaction details and resulting self-assembly structures are influenced by the number and type of substituents. For example, in the case of **3b**, the oxygen (O6) and (O2) of one macrocycle interact with the barbiturate of another macrocycle, leading to four short contacts with four carbonyl groups (Figure S14c). Changing the substituents to mono-ethyl (3c) or geminal-methyl groups (6a) reduced the multiplicity of intermolecular C=O···C=O bonds, with only one C=O···C=O interaction pair observed (Figure S14e, g). In stark contrast to 3a and 3b, the introduction of mono-benzyl groups (3d) facilitates quadruple C=O···C=O interactions with the macrocycle provides one carbonyl oxygen (O5) as the donor and one barbiturate ring (three carbonyl groups) as acceptor (Figure S14i, i). In [2+2] macrocycles, the intermolecular C=O···C=O interactions act as driving forces, leading to the formation of infinite linear self-assemblies (Figure S14b, d, f, h). For larger macrocycles, the increased flexibility of the cavity also modulates the self-assembly structures. For example, the [3+3] macrocycle 7a exhibited different conformations and C=O···C=O interaction motifs depending on the solvent used in crystallization, resulting in chain-like self-assembly (crystallized from dimethylacetamide (DMA) and tetrahydrofuran (THF) mixture) or infinite wave-like self-assembly (crystallized from dichloromethane (CH<sub>2</sub>Cl<sub>2</sub>)) (Figure S15). The [4+4] macrocycle 8a utilizes two barbiturates as the acceptor and donor respectively to form intermolecular C=O···C=O interactions, creating linearly linked porous structures owing to its large cavity (Figure S17).

We selected **6a** and **3c** as representative examples to study the structure of the macrocycles in solution by means of variable-temperature NMR (VT-NMR). While only one set of the NMR signals of **6a** was observed at room temperature in the spectra, two sets of signals corresponding to two conformations (conformations 1 and 2) with an integral ratio of 3:5 appeared when the temperature was below 210 K (Figures S3 and S4). In conformation 1, the aromatic protons al and bl moved to downfield, whereas the methylene protons e1 and e1' shifted to upfield compared to conformation 2. Since a cone conformation results in deshielded aromatic and shielded methylene protons [14], conformation 1 is identified as cone conformation, and conformation 2 as the 1,3-alternate conformation (Figures S5 and S6). The transition between the two conformations likely occurs via the rotation of barbiturate around the C-N bond. In the case of 3c, due to the rotation of the C-N bond and the asymmetrical substitution of the macrocycle, the variation in conformations is more fruitful. Twelve conformations, classified into three groups (a, b, c), could be proposed through C-N bond rotating operations (Figure 2); the conformations within each group a, b, or c are convertible while interconversion between the groups is not possible (Figure S7). To investigate the conformations, we start with a single crystal sample of 3c which adopts a 1,2-alt (in/in) conformation (belonging to group c, Figure 2c). The crystals were dissolved in deuterated dichloromethane (CD<sub>2</sub>Cl<sub>2</sub>) and

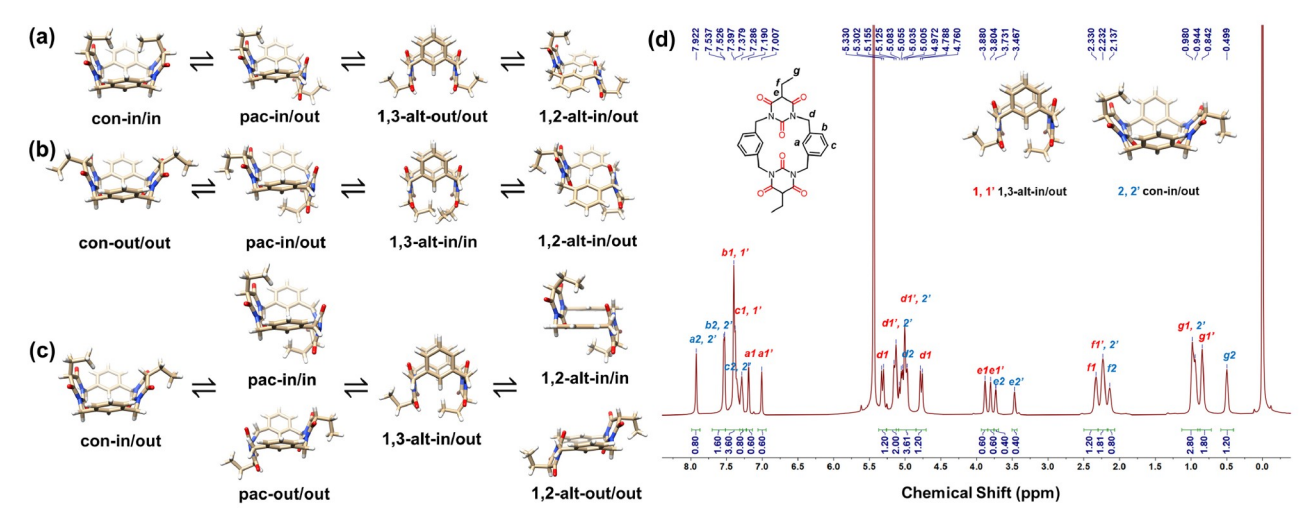


Figure 2 (Color online) Proposed conformations of 3c through C-N bond rotation operations (a-c), <sup>1</sup>H NMR spectra of 3c (in CD<sub>2</sub>Cl<sub>2</sub>) at 190 K (d). Color code: carbon, yellow; oxygen, red; hydrogen, white; nitrogen, blue.

the spectra were recorded at different temperatures (Figure S8). The spectrum recorded at 190 K is shown in Figure 2d. Taking methylene proton e as the indicator, four signals with an integral ratio of 3:3:2:2 were observed, corresponding to two doublets of e. These observations suggest the coexistence of two conformations. Among the conformations illustrated in group c, the 1,2-alt-in/in and 1,2-alt-out/out conformations exhibit  $C_i$ -symmetry, protons e of barbiturate are equivalent and show one indistinguishable signal. Therefore, 1,2-alt-in/in and 1,2-alt-out/out could be excluded as two doublets of e signals (e1 and e1', e2 and e2') in the NMR spectrum are demonstrated. Nuclear Overhauser effect spectroscopy (NOESY) experiments (Figures S9 and S10) revealed a stronger NOE between proton e1' and the methyl proton g1', suggesting a 1,3-alt-in/out conformation as they are spatially close. Additionally, there are NOE signals between the aromatic proton a1' and the methyl proton g1', which occur only in the pac-in/in and 1,3-alt-in/out conformations.

Taken together, the signals of 1 and 1' can be attributed to 1,3-alt-in/out conformation. As no NOE signals between the aromatic protons a2,2' and the methyl protons g2,2' are observed, signals 2 and 2' cannot be assigned to the pac-in/in conformation. On the other hand, the chemical shifts of protons e2,2', f2,2', g2,2' resonate upfield compared to protons e1,1', f1,1', g1,1', while the aromatic protons a2,2', b2,2' resonate at downfield compared to a1,1', b1,1', from which pac-out/out could be excluded. Therefore, signals of 2 and 2' could be assigned to the con-in/out conformation.

After determining the structure of the macrocycles, we next focused on the host-guest complexation properties of the [3+3] and [4+4] macrocycles, as they can provide larger cavities capable of accommodating guest molecules. For example, acetonitrile is included within the cavity of **7a** to produce two CH<sub>3</sub>CN@**7a** complexes (complexes 1 and 2)

[13]. In complex 1, the included acetonitrile induces a  $C_s$ -symmetric partial column conformation of the macrocycle  $(6.9 \times 8.9 \text{ Å})$ , which contrasts sharply with the initially twisted 1,3,5-alternate conformation (vide supra). Examination of the structure indicates that three benzene rings and two barbiturate rings are vertically arranged and encircled, forming the "wall" of the column. The remaining barbiturate ring rotates approximately 90° downward to form the bottom of the column. Moreover, two wall-barbiturates exhibit planar conformations while the bottom one adopts a boat conformation. Acetonitrile is positioned at the center of the column with nitrogen interacting with the electron-deficient centers of the two planar barbiturate rings (Figure 3a). In complex 2, the included acetonitrile within the cavity induces a  $C_{3\nu}$ -symmetric column conformation of the macrocycle. All the benzene and barbiturate rings are nearly vertically aligned along the peripheral wall of the column. The macrocycle exhibits a deep hexagonal cavity with a width around 8.0 Å and a depth around 6.0 Å. Acetonitrile is obliquely inserted into the cavity with nitrogen atom forming N···C=O interactions with one barbiturate ring while the methyl group is surrounded by three benzene rings possibly through van der Waals interactions (Figure 3b). In the case of 8a, two acetone molecules are included within the cavity of 8a, forming acetone<sub>2</sub>@8a complex [13]. Each acetone oxygen forms three C=O···C=O interactions with one barbiturate ring, the interacting O···C=O distances and ∠O···C-O angles are in the range of 2.99-3.28 Å and 110°-122°, respectively (Figure 3c).

The host-solvent complexes clearly demonstrated the ability of carbonyl groups to accept electron-rich species, prompting us to investigate anion binding ability through anion-carbonyl interactions. The study was performed using 7a as the representative host molecule, halide anions and a geometry-complementary malonate as guests. For the NMR

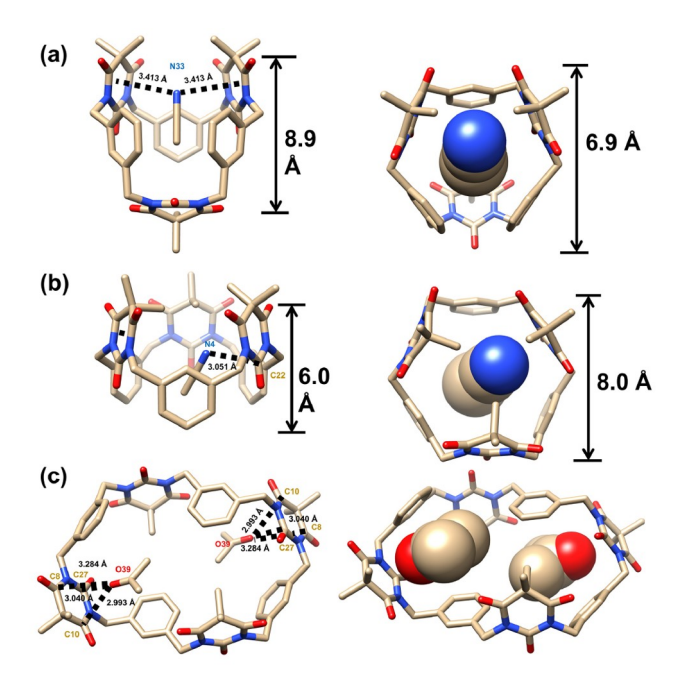


**Figure 3** (Color online) Host-guest complexes of CH<sub>3</sub>CN@**7a** (a, b) and acetone<sub>2</sub>@**8a** (c). Color code: carbon, yellow; oxygen, red; hydrogen, white; nitrogen, blue.

studies, CDCl was employed as the solvent, and tetrabutylammonium salt was used as the cationic species. <sup>13</sup>C NMR titration was employed as a direct technique to reveal anion-carbonyl interactions. We have demonstrated that both electrostatic attraction and  $n\rightarrow\pi^*$  interactions contribute to the attractive energy of anion-carbonyl interactions, the former induces a downfield shift of carbonyl carbon due to the field effect of approaching anions, while the latter causes upfield movement of carbonyl carbon as a result of the delocalization of lone pairs into the antibonding orbital of the carbonyl group in <sup>13</sup>C NMR spectra [12]. As shown in Figure 4, upon the addition of halides, the chemical shifts of carbonyl carbons g and h slightly move downfield, then upfield with fluoride, marginally change with chloride, and continuously shift upfield with bromide and iodide, respectively (Figure S19). The addition of malonate could cause the most significant and continuous upfield shifts of g and h(Figure 4a). Thus, the spectroscopic responses of 7a towards halides result from a combination of competing effects: electrostatic interactions dominate the interactions of 7a with fluoride and chloride, whereas the  $n\rightarrow\pi^*$  interactions prevail over electrostatic attraction in the [7a Br] and [7a I] complexes. In the case of [7a·malonate] complex,  $n\rightarrow\pi^*$ interactions dominate the host-guest complexation. Fitting the titration data using the Bindfit program gives a quantitative binding constant  $(K_{a(1:1)})$  of 13.2  $\pm$  1.57 M<sup>-1</sup> for [7a malonate] complex, which is nearly ten times greater than that of the  $[7a \cdot I^{-}]$  complex  $(1.46 \pm 0.24 \text{ M}^{-1})$ . The stronger association strength of 7a towards malonate is probably due to the geometry and site complementary be-

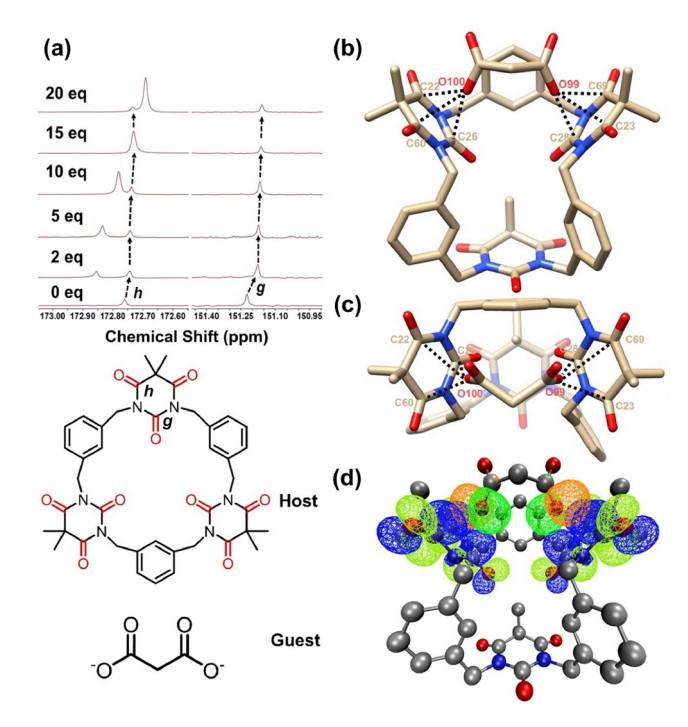


**Figure 4** (Color online) Partial <sup>13</sup>C NMR spectra of **7a** (5 mM, CDCl, 125 MHz) upon the addition of malonate (a), DFT-optimized structure representing multiple anion-carbonyl interactions (dashed black lines) (b, c), and natural bond orbital (NBO) analysis of [**7a**·malonate] complex, showing  $n\rightarrow\pi^*$  contribution (d). Color code: carbon, yellow; oxygen, red; hydrogen, white; nitrogen, blue.

tween host and guest. DFT optimization of the complex confirms the assumption, that malonate is included within the V-shaped cavity formed by two barbiturate rings. Multiple anion-carbonyl interactions between the oxygens of malonate and the carbonyl groups of barbiturate are observed, the  $d_{O-C=O}$  distances ranging from 2.613 to 2.918 Å, and ∠O···C=O angels ranging from 112.50° to 122.60° agree well with the Bürgi-Dunitz trajectory ( $d < \sum v dW$ ,  $\angle O \cdots C = O = 109^{\circ} \pm 10^{\circ}$ ). Furthermore, NBO analysis further confirms significant overlap between the lone pair orbital (n) of the oxygen atoms in malonate and the  $\pi^*$ antibonding orbital of the carbonyl groups, indicating the presence of  $n\rightarrow\pi^*$  interactions. These computational results indicate that  $n\rightarrow\pi^*$  interactions are likely the driving forces behind the selective binding of malonate in solution (Figure 4b, c). The complexes between 7a and anions are also observed in electrospray ionization (ESI) mass spectra (Figures S48-S52).

### 3 Conclusions

In summary, we have successfully synthesized a series of macrocycles using barbiturate rings as functional components. The  $C_3$ -symmetric barbiturate, featuring non-aromaticity and superimposed  $\pi$ -holes or  $\pi^*$  orbitals from three

carbonyl groups at the central region, endows the macrocycles dual-function building blocks for self-assembly. The rationally designed macrocycles with appropriate size cavities, provide convergent and cooperative carbonyl binding sites for anions. The quantification of anion binding through anion-carbonyl interactions in solution has been unprecedentedly demonstrated. This work indicates that anion-carbonyl interactions can be a useful non-covalent driving force for supramolecular chemistry.

**Acknowledgements** This work was supported by the National Natural Science Foundation of China (22371285, 22171271) and the Beijing National Laboratory for Molecular Sciences (BNLMS-CXXM-202002).

Conflict of interest The authors declare no conflict of interest.

**Supporting information** The supporting information is available online at <a href="http://chem.scichina.com">http://chem.scichina.com</a> and <a href="http://link.springer.com/journal/11426">http://chem.scichina.com</a> and <a href="http://link.springer.com/journal/11426">http://link.springer.com/journal/11426</a>. The supporting materials are published as submitted, without typesetting or editing. The responsibility for scientific accuracy and content remains entirely with the authors.

- (a) Lehn JM. Supramolecular Chemistry: Concepts and Perspectives. Weinheim: VCH Verlagsgesellschaft mbH, 1995; (b) Steed JW, Atwood JL. Supramolecular Chemistry (second edition). Chichester: John Wiley & Sons, Ltd., 2009; (c) Gale PA, Sessler JL, Král V, Lynch V. J Am Chem Soc, 1996, 118: 5140–5141; (d) Ogoshi T, Kanai S, Fujinami S, Yamagishi T, Nakamoto Y. J Am Chem Soc, 2008, 130: 5022–5023; (e) Lagona J, Mukhopadhyay P, Chakrabarti S, Isaacs L. Angew Chem Int Ed, 2005, 44: 4844–4870; (f) Chen Y, Liu Y. Chem Soc Rev, 2010, 39: 495–505
- 2 Neri P, Sessler J L, Wang M X. Calixarenes and Beyond. Cham: Springer, 2016
- 3 (a) Dougherty DA. Acc Chem Res, 2013, 46: 885–893; (b) Macias AT, Norton JE, Evanseck JD. J Am Chem Soc, 2003, 125: 2351–2360
- 4 (a) Gropp C, Quigley BL, Diederich F. J Am Chem Soc, 2018, 140: 2705–2717; (b) Pancholi J, Beer PD. Coord Chem Rev, 2020, 416: 213281; (c) Mullaney BR, Thompson AL, Beer PD. Angew Chem Int Ed, 2014, 53: 11458–11462; (d) Zhao T, Lynch VM, Sessler JL. Org Biomol Chem, 2022, 20: 980–983; (e) Vargas Jentzsch A, Emery D, Mareda J, Metrangolo P, Resnati G, Matile S. Angew Chem, 2011, 123: 11879–11882
- 5 (a) Lim JYC, Marques I, Thompson AL, Christensen KE, Félix V, Beer PD. J Am Chem Soc, 2017, 139: 3122–3133; (b) Chen L, Xiang J, Zhao Y, Yan Q. J Am Chem Soc, 2018, 140: 7079–7082; (c) Rahman FU, Tzeli D, Petsalakis ID, Theodorakopoulos G, Ballester P, Rebek Jr. J, Yu Y. J Am Chem Soc, 2020, 142: 5876–5883; (d) Riwar L, Trapp N, Root K, Zenobi R, Diederich F. Angew Chem Int Ed, 2018, 57: 17259–17264
- 6 (a) Wang DX, Wang MX. Acc Chem Res, 2020, 53: 1364-1380;

- (b) Escobar L, Sun Q, Ballester P. Acc Chem Res, 2023, 56: 500–513
  (a) Paulini R, Müller K, Diederich F. Angew Chem Int Ed, 2005, 44: 1788–1805; (b) Singh SK, Das A. Phys Chem Chem Phys, 2015, 17: 9596–9612; (c) Newberry RW, Raines RT. Acc Chem Res, 2017, 50: 1838–1846; (d) Sahariah B, Sarma BK. Phys Chem Chem Phys, 2020, 22: 26669–26681
- (a) Bretscher LE, Jenkins CL, Taylor KM, DeRider ML, Raines RT. J Am Chem Soc, 2001, 123: 777-778; (b) DeRider ML, Wilkens SJ, Waddell MJ, Bretscher LE, Weinhold F, Raines RT, Markley JL. J Am Chem Soc, 2002, 124: 2497-2505; (c) Bartlett GJ, Choudhary A, Raines RT, Woolfson DN. Nat Chem Biol, 2010, 6: 615-620; (d) Khatri B, Majumder P, Nagesh J, Penmatsa A, Chatterjee J. Chem Sci, 2020, 11: 9480-9487; (e) Erdmann RS, Wennemers H. J Am Chem Soc, 2012, 134: 17117-17124; (f) León I, Alonso ER, Cabezas C, Mata S, Alonso JL. Commun Chem, 2019, 2: 3; (g) Hoang HN, Wu C. Hill TA. Dantas de Araujo A. Bernhardt PV. Liu L. Fairlie DP. Angew Chem Int Ed, 2019, 58: 18873-18877; (h) Umashankara M, Sonar MV, Bansode ND, Ganesh KN. J Org Chem, 2015, 80: 8552-8560; (i) Gorske BC, Bastian BL, Geske GD, Blackwell HE. J Am Chem Soc, 2007, 129: 8928–8929; (j) Harris T, Chenoweth DM. J Am Chem Soc. 2019. 141: 18021–18029: (k) Chen H. Tang X. Ye H. Wang X, Zheng H, Hai Y, Cao X, You L. Org Lett, 2021, 23: 231-235; (1) Wang H, Kohler P, Overman LE, Houk KN. J Am Chem Soc, 2012, 134: 16054-16058; (m) Vik EC, Li P, Pellechia PJ, Shimizu KD. J Am Chem Soc, 2019, 141: 16579-16583; (n) Sonntag LS, Schweizer S, Ochsenfeld C, Wennemers H. J Am Chem Soc, 2006, 128: 14697-14703; (o) Fischer F, Schweizer W, Diederich F. Angew Chem Int Ed, 2007, 46: 8270-8273; (p) Rahim A, Sahariah B, Sarma BK. Org Lett, 2018, 20: 5743-5746; (q) Polaske NW, Nichol GS, Szabó LZ, Olenyuk B. Cryst Growth Des, 2009, 9: 2191-2197
- 9 (a) Choudhary A, Fry CG, Kamer KJ, Raines RT. *Chem Commun*, 2013, 49: 8166–8168; (b) Ni C, Zha D, Ye H, Hai Y, Zhou Y, Anslyn EV, You L. *Angew Chem Int Ed*, 2018, 57: 1300–1305; (c) Neveselý T, Molloy JJ, McLaughlin C, Brüss L, Daniliuc CG, Gilmour R. *Angew Chem Int Ed*, 2022, 61: e202113600
- 10 Zheng H, Ye H, Yu X, You L.  $\it JAm \ Chem \ Soc$ , 2019, 141: 8825–8833
- (a) Zhu J, Wang X, Ao Y, Wang Q, Wang D. *Chem Eur J*, 2023, 29: e202203485;
   (b) Singh SK, Mishra KK, Sharma N, Das A. *Angew Chem Int Ed*, 2016, 55: 7801–7805;
   (c) Dutta J, Routray C, Pandey S, Biswal HS. *Chem Sci*, 2022, 13: 14327–14335;
   (d) Wang W, Li X, Zhou PP, Wang Y. *Angew Chem*, 2021, 133: 22899–22903
- 12 Zhu J, Tuo DH, Wang XD, Ao YF, Wang QQ, Wang DX. Org Lett, 2024, 26: 5984–5988
- 13 Deposition Numbers 2416969–2416980 and 2416935 contain the supplementary crystallographic data for this paper. These data are provided free of charge by the joint Cambridge Crystallographic Data Centre and Fachinformationszentrum Karlsruhe Access Structures service www.ccdc.cam.ac.uk/structures
- 14 Gutsche CD, Dhawan B, Levine JA, Hyun No K, Bauer LJ. *Tetra-hedron*, 1983, 39: 409–426
- 15 Huo H, Xiao X, Chang L, Xiong X, Shi M, Wang J, Tian W. Sci China Chem, 2023, 66: 2070–2082
- 16 Xia N, Zhao J, Gong G, Dong H, Li H, Wang J, Wang L, Chen S. Sci China Chem, 2023, 66: 3169–3177